TECHNICAL MEMORANDUM

607

New snow scheme in HTESSEL: description and offline validation

E. Dutra[1,2], G. Balsamo[3], P. Viterbo[4], P.M.A Miranda[1], A. Beljaars[3], C. Schär[2], and K. Elder[5]

Research Department

[1]CGUL,IDL, University of Lisbon, Portugal
[2]IAC, ETH Zurich, Switzerland
[3] ECMWF, England
[4]Instituto de Meteorologia, Lisbon, Portugal
[5] Rocky Mountain Research Station, USDA Forest Service, USA

December 2009

Submitted to Journal of Hydrometeorology

European Centre for Medium-Range Weather Forecasts
Europäisches Zentrum für mittelfristige Wettervorhersage
Centre européen pour les prévisions météorologiques à moyen

Series: ECMWF Technical Memoranda

A full list of ECMWF Publications can be found on our web site under:
http://www.ecmwf.int/publications/

Contact: library@ecmwf.int

European Centre for Medium Range Weather Forecasts
Shinfield Park, Reading, Berkshire RG2 9AX, England

Abstract

A new snow scheme for the European Centre for Medium-Range Weather Forecasts (ECMWF) land surface model has been tested and validated. The scheme includes a new parameterization of snow density, incorporating a liquid water reservoir, and revised formulations for the sub-grid snow cover fraction and snow albedo. Offline validation (covering a wide range of spatial and temporal scales) includes simulations for several observation sites from the Snow Models Intercomparison Project-2 (SnowMIP2), global simulations driven by the meteorological forcing from the Global Soil Wetness Project-2 (GSWP2), and by ECMWF ERA-Interim re-analysis. The new scheme reduces the end of season ablation biases from 10 to 2 days in open areas, and from 21 to 13 day in forest areas. Global GSWP2 results are compared against basin scale runoff and terrestrial water storage. The new snow density parameterization increases the snow thermal insulation, reducing soil freezing and leading to an improved hydrological cycle. Simulated snow cover fraction is compared against NOAA/NESDIS with a reduction of the negative bias of snow-covered area of the original snow scheme. The original snow scheme had a systematic negative bias in surface albedo, when compared against MODIS remote sensing data. The new scheme reduces the albedo bias, consequently reducing the spatial and time averaged surface net shortwave radiation bias by 5.2 W m^{-2} in 14% of the northern hemisphere land. The new snow scheme described in this report was introduced in the ECMWF operational forecast system in September 2009 (CY35R3).

1 Introduction

The extent and variability of snow cover are important parameters in weather and climate prediction systems, due to their effects on energy and water balances, justifying a strong dependency of surface temperature on the presence or absence of snow cover (Armstrong and Brun 2008). Eurasian snow cover has been linked with the variability of the Indian summer monsoon (Douville and Royer 1996; Liu and Yanai 2002; Robock et al. 2003), and with significant changes in the hemispheric circulation (Cohen et al. 2007; Gong et al. 2007; Fletcher et al. 2009). Snow cover also acts as a water reservoir, which is released by snowmelt in spring, influencing runoff, soil moisture, evaporation, and thus precipitation and the entire hydrological cycle (e.g., Douville et al. 2002; Groisman et al. 2004). Therefore, an accurate simulation of snow processes is essential for many applications ranging from hydrological forecast to numerical weather prediction (NWP) and seasonal and climate modeling. Observed climate change during the 20th century, particularly visible in the northern hemisphere surface warming in spring, has been significantly enhanced by the associated depletion of snow cover (Groisman et al. 1994a).

The presence of snow modulates the exchanges between the atmosphere and the surface. When compared with other natural surfaces, snow is remarkable in three different ways: an anomalously high albedo, an anomalously low thermal conductivity, and the ability of change phase (sometimes leading to co-existing liquid and solid water revervoirs). High surface albedo in the presence of snow causes rapid shifts in surface reflectivity in autumn and spring at high latitudes. Viterbo and Betts (1999) showed that changing the albedo of boreal forest in the presence of snow in the European Centre for Medium-Range Weather Forecasts (ECMWF) model reduced the model systematic cold bias at the surface at high northern latitudes in spring. Changes in the snow cover fraction and in its sub-grid scale variability are largely responsible for the observed interannual variability of surface albedo (Roesch and Roeckner 2006). On the other hand, the large amount of energy required to melt ice means that snow retards warming during the melting period. When melting occurs but is incomplete, liquid water may remain in the snowpack, significantly changing its properties and allowing for later refreezing. Because of that, the representation of a heterogeneous snowpack is important (Rutter et al. 2008), as are the effects of incident rainfall on the energy and mass balances (Bélair et al. 2003). The thermal insulation property of snow also has important climatic consequences. Cook

et al. (2008) evaluated the impact of snow thermal conductivity in a climate model, reporting changes in soil temperature up to 20 K and in the air temperature up to 6 K during winter, just by prescribing snow thermal conductivity to its observed upper and lower limits. Grippa et al. (2005) showed that later snowmelt dates and thicker winter snowpacks are related to higher Normalized Difference Vegetation Index (NDVI) values over a large latitudinal band of about 65°N. The authors suggested that this could be related by either an increased water availability for plants after snowmelt, or thermal insulation of the soil by snow.

Snow parameterizations in land surface models (LSM) used in NWP, climate modeling, and in various applications such as hydrological forecasting or avalanche prediction, vary greatly in complexity. Boone and Etchevers (2001) divided snow schemes in three general categories according to their complexity: 1) simple force-restore or single explicit snow layer schemes (Verseghy 1991; Douville et al. 1995; Yang et al. 1997; Slater et al. 1998); 2) detailed internal-snow-process schemes (Anderson 1976; Brun et al. 1989; Jordan 1991) and; 3) intermediate-complexity schemes based on class 2) but using simplified versions of the physical parameterizations (Loth et al. 1993; Lynch-Stieglitz 1994; Sun et al. 1999; Boone and Etchevers 2001). The Hydrology Tiled ECMWF Scheme of Surface Exchanges over Land (HTESSEL, Viterbo and Beljaars 1995; van den Hurk et al. 2000; Balsamo et al. 2009) included in the ECMWF model has a simple snow scheme, laying within the first category, with an explicit snow layer similar to the schemes described in Verseghy (1991) and Douville et al. (1995).

The different treatment of snow processes in LSMs has been demonstrated in several offline LSM intercomparison experiments. TESSEL (a previous version of the model, but with the same snow scheme) participated in the Thorne-Kalix experiment (Nijssen et al. 2003, van den Hurk and Viterbo 2003), the Rhone Aggregation experiment (Boone et al. 2004), and the Snow Models Intercomparison Project-2 (SnowMIP2) (Essery et al. 2009; Rutter et al. 2009). Initial results of TESSEL in SnowMIP2 revealed some model weaknesses, motivating the development of the revised snow model described in the present report.

The present work describes a revision of HTESSEL's snow scheme and its validation. The snow scheme revision includes four main processes: i) representation of liquid water content as a diagnostic, following a similar approach applied to soil phase changes by Viterbo et al. (1999); ii) new snow density parameterization following Anderson (1976) and Boone and Etchevers (2001); iii) revised snow cover fraction, and iv) revision of exposed snow albedo and new forest albedo in the presence of snow adapted from Moody et al (2007). The changes to the model (section 2) were performed keeping the same level of complexity (single explicit snow layer). This constraint allowed a simple integration with the ECMWF integrated forecast system (IFS) in its several applications ranging from data assimilation for short-range weather forecast to seasonal prediction. Offline validation covering several spatial and temporal scales considered (i) site simulations for several observation locations from SnowMIP2 (section 3), and (ii) global simulations driven by the meteorological forcing from the Global Soil Wetness Project 2 (GSWP2) (Dirmeyer et al. 1999; Dirmeyer et al. 2002; Gao et al. 2004) and by ECMWF ERA-Interim re-analysis (hereafter ERAI) (Simmons et al. 2007). GSWP2 Results are compared against basin scale runoff and terrestrial water storage variation (TWSV) in section 4. In Section 5 ERAI simulated snow cover fraction and surface albedo are compared with remote sensed products. Model results are presented and discussed throughout the text and the main conclusions of the work are summarized in section 6.

2 Models

2.1 HTESSEL

HTESSEL represents vertical transfers of water and energy using four vertical layers to represent soil temperature and moisture. The model evaluates the land surface response to the atmospheric forcing, and estimates the surface water and energy fluxes along with the temporal evolution of the snowpack, soil temperature and moisture. At the interface between the surface and the atmosphere, each grid-box is divided into fraction (tiles), with up to six fractions over land (bare ground, low and high vegetation, intercepted water, shaded and exposed snow). Each fraction has its own properties defining separate heat and water fluxes used in the energy balance equation solved for the tile skin temperature. The snow scheme in HTESSEL is an energy- and mass-balance model that represents an additional layer on top of the upper soil layer, with independent prognostic thermal and mass contents. The formulation of the snow mass (or snow water equivalent – SWE) and energy budgets in HTESSEL are described in the appendix along with the snow density and albedo parameterizations.

2.1.1 Revised snow scheme

a) Snow liquid water content

The HTESSEL snow scheme does not account for snow liquid water (SLW hereafter) in the snowpack (see appendix). A proper consideration of the SLW requires several modifications: (i) the thermal effects related to the latent heat of fusion (Tribbeck et al. 2006); (ii) changes in the snow runoff (following Rutter et al. (2008), as opposed to the current scheme in which melted snow leaves the snowpack immediately), and; (iii) interception of rainfall by the snowpack (as in Bélair et al. 2003) correcting for the rainfall bypass of the snowpack in the current scheme).

The snow energy budget (eq. A.4) in the presence of SLW changes can be written as

$$\begin{aligned} \left(\rho C\right)_{sn} D_{sn} \frac{\partial T_{sn}}{\partial t} &= R_{sn}^{N} - L_s E_{sn} - H_{sn} - G_{sn}^{B} - L_f M_{sn} - Q_{sn}^{INT} \\ Q_{sn}^{INT} &= L_f M_{sn}^{INT} = L_f \frac{\partial S_l}{\partial t} \end{aligned} \tag{1}$$

where $\left(\rho C\right)_{sn}$ is the snow volumetric heat capacity (J m^{-3} K^{-1}), D_{sn} is the snowpack depth (m), T_{sn} is the snow temperature (K) , and the energy fluxes R_{sn}^{N}, H_{sn} and G_{sn}^{B} are the net radiation (shortwave and longwave), sensible heat flux and basal heat flux (W m^{-2}), respectively. The mass fluxes E_{sn} and M_{sn} are the snow sublimation and melting (kg m^{-2} s^{-1}), respectively, that are associated with the latent heat of sublimation L_s and fusion L_f (J kg^{-1}). The superscript *INT* denotes internal phase changes, where Q_{sn}^{INT} is the heat change associated with internal phase changes, and S_l is the snow liquid water content (SLW) (kg m^{-2}). Without loss of generality, it can be assumed that for the grid squares characteristic of NWP,

$$S_l = S_l\left(T_{sn}, S\right) \approx f\left(T_{sn}\right) S_l^c\left(S, \rho_{sn}\right) \tag{2}$$

where S_l^c (kg m^{-2}) is the snow liquid water capacity, S (kg m^{-2}) is the sum of snow and water in the snowpack (also referred as SWE along the text) and ρ_{sn} is the snow density (kg m^{-3}). The snow temperature function is

prescribed in an analytical form – following a similar approach described by Viterbo et al. (1999) for soil phase changes

$$f\left(T_{sn}\right)=\begin{cases}0 & ,T_{sn}<T_f-d/2\\ 1+\sin\left(\dfrac{\pi\left(T_{sn}-T_f\right)}{d}\right) & ,T_{sn}\geq T_f-d/2\end{cases} \tag{3}$$

where T_f is the triple-point temperature for water (273.16 K) and d is a characteristic temperature difference, in respect to T_f, limiting the phase change regime. In the numerical implementation d = 4 K was chosen. Snow liquid water capacity is approximated as a function of SWE and snow density, following Anderson (1976)

$$S_l^c = S\left[r_{l,\min}+\left(r_{l,\max}-r_{l,\min}\right)\max\left(0,\rho_{sn,l}-\rho_{sn}\right)/\rho_{sn,l}\right] \tag{4}$$

with the constants $r_{l,min}$=0.03, $r_{l,max}$=0.1 and $\rho_{sn,l}$=200 kg m^{-3}. This equation is a simple parameterization of a very complex phenomena, and has been used recently in other snow schemes for NWP, e.g. Boone and Etchevers (2001).

Combining equations (1) and (2) results in a modified snow energy budget equation

$$\left[\left(\rho C\right)_{sn}D_{sn}+L_f S_l^c\frac{\partial f\left(T_{sn}\right)}{\partial T_{sm}}\right]\frac{\partial T_{sn}}{\partial t}=R_{sn}^N-L_sE_{sn}-H_{sn}-G_{sn}^B-L_fM_{sn} \tag{5}$$

with one extra term in the l.h.s. of the equation, that can be interpreted as an additional snow heat capacity – or heat capacity barrier. In compacted snowpacks, the representation of SLW as a diagnostic increases the snow heat capacity by a factor of five (see Fig 1a). This increase acts as a heat-barrier near T_f, representing the increased snow temperature inertia due to freeze-melt events.

This diagnostic approach for SLW also allows the representation of rainfall interception. The new snow mass balance read as

$$\frac{\partial S}{\partial t}=F+c_{sn}F_l-c_{sn}E_{sn}-R_{sn} \tag{6}$$

where F, F_l and R_{sn} are the mass fluxes of snowfall, rainfall and runoff (kg m^{-2} s^{-1}) and c_{sn} is the snow cover fraction. Rainfall is considered to reach the snowpack at T_f, and the latent heat released by the freezing of the intercepted rainfall, if $T_{sn}<T_f$, is also accounted in the energy balance solution. Runoff is defined has the rate at which liquid water leaves the snowpack and parameterized as follows:

$$R_{sn}=c_{sn}M_{sn}+\max\left(c_{sn}F_l-\frac{S_l^c\left(1-f\left(T_{sn}\right)\right)}{\Delta t},0\right) \tag{7}$$

Liquid water is generated by melting (M_{sn}) and by rainfall interception (F_l). When snow liquid water content exceeds the snow liquid water capacity (defined in eq. 4) runoff is generated.

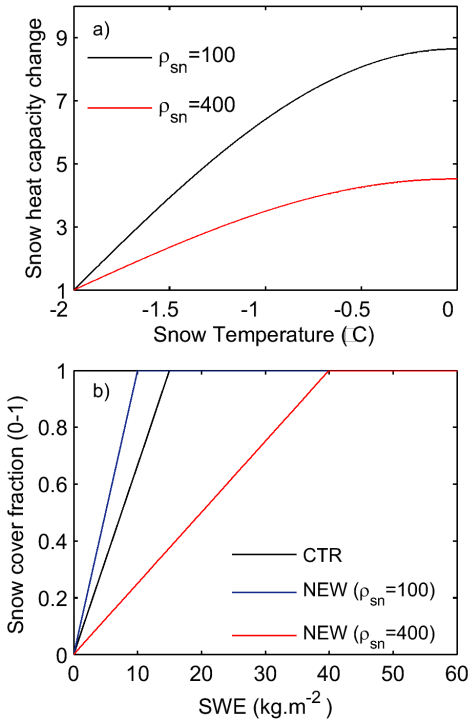

Fig 1. a) Ratio between the apparent snow heat capacity (l.h.s of eq.5) and snow heat capacity, as function of snow temperature for constantan SWE of 100 kg.m^{-2} and snow densities of 100 (black), and 400 (red) kg.m^{-3}. b) Snow cover fraction as function of SWE as in the original HTESSEL snow scheme (black – eq.A.3), and new (eq. 12) for snow densities of 100 (blue) and 400 (red) kg.m^{-3}.

b) Snow density

The rate of density change is parameterized as

$$\frac{1}{\rho_{sn}}\frac{\partial \rho_{sn}}{\partial t} = \frac{\sigma_{sn}}{\eta_{sn}\left(T_{sn},\rho_{sn}\right)} + \xi_{sn}\left(T_{sn},\rho_{sn}\right) + \frac{\max\left(0,Q_{sn}^{INT}\right)}{L_f\left(S-S_l\right)} \tag{8}$$

where the first two terms represent overburden and thermal metamorphism (Anderson 1976, Boone and Etchevers 2001), respectively, and the last term represents the compaction related to melt water retained in the snowpack, adapted from Lynch-Stieglitz (1994). In the overburden term (first term on the r.h.s of eq. 8) σ_{sn} and η_{sn} are the pressure of the overlying snow (Pa) and snow viscosity (Pa s), respectively. Melted water retained in the snowpack leads to a decrease of snow depth, while keeping the SWE constant. Following the original scheme, a weighted average is taken between the current snow density and the density of snowfall. Snowfall density is changed from a constant value to an expression from CROCUS (Brun et al. 1989; Brun et al. 1992) were fresh snow density is a function of near surface air temperature and wind speed

$$\rho_{new} = a_{sn} + b_{sn}(T_{air} - T_f) + c_{sn}(V_a)^{1/2} \tag{9}$$

where T_{air} and V_a are the near surface air temperature (K) and wind speed (m s^{-1}), respectively. The coefficients are a_{sn}=109 kg m^{-3}, b_{sn}=6 kg m^{-3}, and c_{sn}=26 kg m$^{-7/2}$ s$^{1/2}$. Snow density is constrained to be between 50 to 450 kg m^{-3}.

The snow viscosity is formulated following Anderson (1976) as

$$\eta_{sn} = \eta_0 \exp\left(a_\eta \left(T_f - T_{sn}\right) + b_\eta \rho_{sn}\right) \tag{10}$$

where η_0=3.7 × 10^7 Pa s, a_η=8.1 ×10^{-2} K^{-1} and b_η=1.8×10^{-2} m^3 kg^{-1}. The pressure of the overlying snow is given by $\sigma_{sn} = \frac{1}{2} S \times g$, where g is the standard gravity (m^2 s^{-2}).

The thermal metamorphism (second term on the r.h.s. of eq. 8) is parameterized as

$$\xi_{sn} = a_\xi \exp\left[-b_\xi \left(T_f - T_{sn}\right) - c_\xi \max\left(0, \rho_{sn} - \rho_\xi\right)\right] \tag{11}$$

using the constant values of Anderson (1976): a_ξ = 2.8×10^{-6} s^{-1}, b_ξ = 4.2×10^{-2}, c_ξ = 460 m^3 kg^{-1}, and ρ_ξ = 150 kg m^{-3}.

c) Snow cover fraction

The new formulation for snow cover fraction depends on both SWE and snow density

$$c_{sn} = \min\left(1, \frac{S/\rho_{sn}}{0.1}\right) \tag{12}$$

This new formulation, although very simple, is expected to represent the hysteresis of snow cover between the beginning of the cold season (low snow densities) and the later stage of ablation (high snow densities). In the beginning of the cold season a reduced amount of SWE is needed to fully cover an entire grid-box. During the ablation period, the emergence of snow-free patches reflects the need of much more SWE to have a fully-covered grid-box. Figure 1b shows the different paths of snow cover fraction as function of SWE for a low and high density snowpack. The original scheme (Eq.A.2) lies between the two extremes of snow densities.

d) Snow albedo

Snow albedo in exposed areas evolves according to the original scheme (see Eq. A.6) with two differences. The melting formulation for albedo decay is also activated when $T_{sn} \geq T_f - 2$. The representation of SWL as a diagnostic (see Eqs. 1,2 and 3) is also activated, with internal phase changes, above this temperature threshold. The definition of this temperature threshold for both SLW and albedo decay also accounts for the sub-grid scale variability of the snowpack properties for typical climate and NWP resolutions.

The original snow albedo in exposed areas was reset to is maximum value when F > 1 kg m^{-2} hr^{-1}. This threshold, and its definition, has been reported as a drawback in this type of snow albedo parameterization (Pedersen and Winther 2005; Molders et al. 2008) also used in other NWP models. In order to reduce the importance of the threshold a continuous reset was implemented

$$\alpha_{sn}^{t+1} = \alpha_{sn}^{t} + \min\left(1, \frac{F\Delta t}{10}\right)\left(\alpha_{max} - \alpha_{sn}^{t}\right) \tag{13}$$

where α_{sn} is the snow albedo. Superscripts t and t+1 represent the current and next time step, respectively, and Δt is the model time step (s). This formulation assumes that 10 kg m^{-2} of fresh snowfall are needed to reset the snow albedo to its maximum value (α_{max}=0.85).

The albedo of shaded snow (snow under high vegetation) was changed from a constant value of 0.15 to a vegetation type dependent albedo (see table 1) adapted from Moody et al. (2007). Moody et al. (2007) provide a five-year (2000-2004) climatological statistics of Northern Hemisphere broadband (0.3-5.0 μm) white-sky albedo for the 16 International Geosphere-Biosphere Program (IGBP) ecosystem classes when accompanied by the presence of snow on the ground. The statistics were obtained using validated, high quality Moderate Resolution Imaging Spectroradiometer (MODIS) land surface albedo data, flagged as snow in the associated quality assurance fields. The re-tuned forest albedo towards significantly higher values accounts implicitly for trees intercepted snow effect, which is neglected in the current scheme.

Table 1. Mean values of Northern Hemisphere five-year (2000-2004) broad band surface albedo (in presence of snow) aggregated by high vegetation type (adapted from Moody et al. 2007)

Index	Vegetation type	Albedo
3	Evergreen needle leaf trees	0.27
4	Deciduous needle leaf trees	0.33
5	Deciduous broad leaf trees	0.31
6	Evergreen broad leaf trees	0.38
18	Mixed forest / woodland	0.29
19	Interrupted forest	0.29

3 Site validation

3.1 Simulation setup and observations

Different sets of experiments were performed (see table 2). These experiments include the original (CTR) and new (NEW) snow schemes and intermediate model configurations with progressive activation of the described changes to the model. All the activated parameterizations were described in the previous section except LWPR and NEW_PR (table 2). In those two experiments SLW is represented using a prognostic approach. In this approach a new prognostic equation for SLW was implemented following very simple assumptions: i) SLW only coexists with ice when $T_{sn}=T_f$; ii) melted snow goes to the SLW reservoir with maximum capacity defined by eq. (4); and iii) snow runoff is generated when the amount of SLW exceeds the liquid water holding capacity. This parameterization is not described in detail since its formulation is not essential to the discussion.

HTESSEL, with its original snow scheme, participated in the SnowMIP2 intercomparison project. Rutter et al. (2009) and Essery et al. (2009) report the main conclusions of the project along with information regarding the different observational sites, which included five locations with data in both open and forest sites for two winter seasons: Alptal (47°3N, 8°43E, 1200 m, Switzerland); BERMS (53°55N, 104°42W, 579 m, Canada); Fraser (39°53N, 105°53W, 2820 m, USA); Hitsujigaoka (39°53N, 105°53W, 2820 m, Japan, only one winter); and Hyytiälä (61°51N, 24°17E, 181 m, Finland). Near-surface atmospheric forcing data were available for all locations and observations include snow depth, snow density and SWE. Simulations were performed for all five SnowMIP2 locations summing a total of 18 different cold seasons×sites. Initial conditions and climatological data were made available by the data providers.

Table 2. Sensitivity experiments acronyms and respective activated parameterizations

Experiment	Activated parameterizations
CTR	(see appendix for description)
DENS	snow density (eq. 8)
LWD	snow density + siquid water diagnostic (eq. 5 + eq. 6 setting $F_{l,sn}$=0
LWDR	LWD + rainfall interception (eq. 6)
LWDR_A	LWDR + exposed snow albedo (eq. 13)
LWDR_FA	LWDR + forest snow albedo (table 1)
LWDR_AFA	LWDR + exposed snow albedo (eq. 13) + forest snow albedo (table 1)
LWDR_SC	LWDR + snow cover fraction (eq. 12)
NEW	LWDR_AFA + snow cover fraction (eq. 12)
[a]LWPR	Snow density + liquid water prognostic + rainfall interception
[a]NEW_PR	LWPR + exposed snow albedo + forest snow albedo + snow cover fraction
[a]-Prognostic representation of snow liquid water content	

The results of TESSEL presented in Essery et al. (2009) are not identical to the CTR results presented in this report. The model has the same snow and soil hydrology, but the surface roughness lengths were changed from input fields to land cover type dependent. In the present report, all the simulations were performed with the revised roughness lengths. That modification improved the simulations over forested areas. The changes are prior to the development of the new snow scheme, and due to its different physical and technical nature, they are not described or discussed here.

3.2 Snow depth, density and SWE

Model results and observations of SWE, snow depth, and snow density for the 2004-05 winter season in the Fraser open and forest sites are shown in Fig. 2. CTR and NEW underestimate SWE (Fig. 2a,d) from the beginning of the winter season throughout mid spring in both forest and open sites suggesting either too much melting or excessive sublimation. During the ablation period, CTR showed an early melting in the forest site (Fig. 2a), and a late melting in the open site (Fig. 2d). These distinct errors between open and forest sites during the ablation period were also observed in other SnowMIP2 locations (not shown). Averaged for all 18 CTR simulations, the final ablation is delayed by 10 days and accelerated by 21 days in open and forest sites, respectively. The NEW snow scheme prediction of final ablation is closer to observations with an average delay of 2 days in open sites and an acceleration of 13 day in forest sites.

Figure 2c,f compare simulated versus observed snow density. Snow density is overestimated by CTR throughout the winter season until the final ablation period when it is underestimated. The simulations show a fast (exponential – see eq. A.5) density increase in the beginning of the winter, keeping snow density close to its maximum value of 300 kg m^{-3} during the remaining cold season. This behavior was observed in all available locations. The NEW snow density is closer to the observations representing the low densities during the accumulation stage and the fast increase in the final ablation. Snow depth in CTR and NEW was underestimated in both sites (Fig. 2 b,e), resulting from the SWE underestimation. However, NEW snow depth has a reduced error, when compared with CTR, due to the significant improvement of snow density.

3.3 Snow and soil temperature

Simulated snow and soil temperatures at the Fraser open site during the 2004-05 winter are compared against observations in figure 3. Observations of snow temperature were conducted using a thermocouple string at fixed depths, every 10 cm up to 180 cm. Mean snowpack temperature was derived by averaging the thermocouple observations covered by snow, where snow depth was measured using an acoustic sensor. The

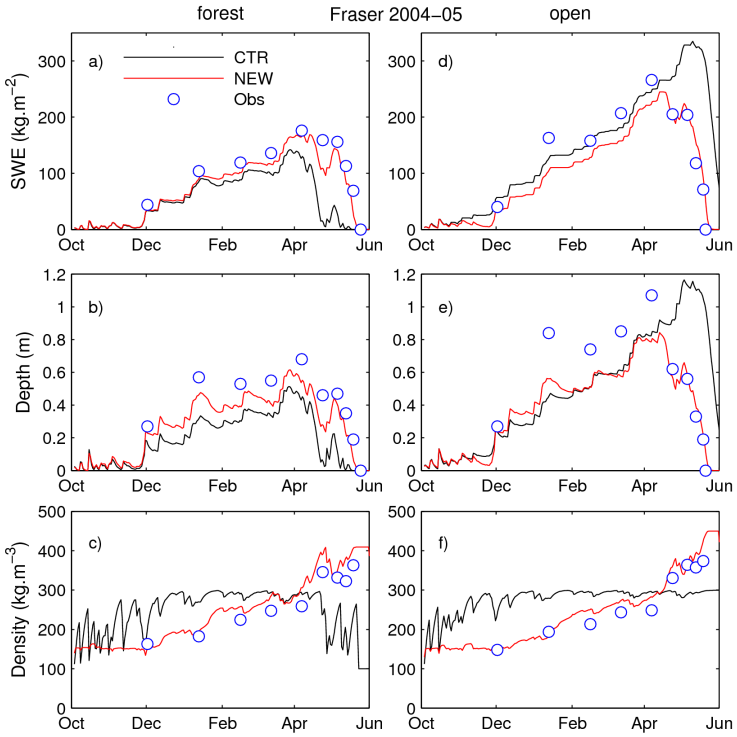

Fig 2. Simulations results for CTR (in black) and NEW (in red) for the 2004-05 winter season at Fraser forest (left) and open (right) sites: SWE (a, d), snow depth (b, e) and snow density (c, f). Observations are represented by open circles.

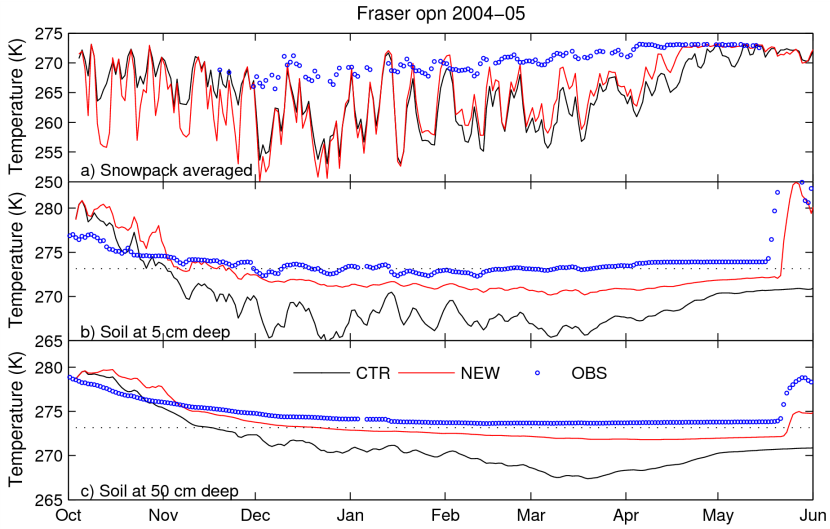

Fig. 3 Model-simulated snow temperature (a) and soil layer temperature at 5 cm depth (b) and 50 cm depth (c) by CTR (in black) and NEW (in red) for the 2004-05 winter season in Fraser open site. The simulations and observations (open circles) represent daily means.

observed mean snowpack temperature (Fig 3a) has a lower thermal amplitude than CTR and NEW, and both simulations underestimate snow temperature throughout the cold season. In a single layer snow scheme it isnot possible to represent properly the thermal insulation within the snowpack. This explains the differences between simulated and observed mean snowpack temperature. However, at the end of the cold season, NEW reaches the freezing point faster than CTR and stays in an isothermal state, as the observations suggest, while CTR shows some cooling cycles.

Simulated soil temperatures respond to the different basal heat fluxes, due to the increase isolation in NEW, with a faster cooling in CTR when compared with NEW (Fig. 3bc). This behavior is observed both near the surface and at 50 cm deep. Averaged from December to mid May CTR has a negative bias of -5.2 and -3.9 K at 5 and 50 cm deep, respectively. NEW reduces significantly the soil temperature bias to -1.8 and -1.3 K at 5 and 50 cm deep, respectively. NEW improves the prediction of final ablation (see Fig. 2d) which affects soil heating after snow disappearance. There is a reduction of the soil temperature bias near the surface by the end of May from -11.4 K in CTR to -2.8 K in NEW.

3.4 Sensitivity to activated parameterizations

Sensitivity tests, where the components of NEW were gradually activated, are detailed in table 2. The comparison was made to the root mean square errors (RMSE) in modeled SWE normalized by standard deviations of the observations (errors in snow depth, rather than SWE, were calculated for Hitsujigaoka and Hyytiälä open sites). Figure 4 summarizes the RMSE for all locations classified as open (Fig. 4a) or forest (Fig. 4b) sites. The new snow density (DENS) has a limited impact on SWE simulation, whereas when combined with SLW representation (LWD) improves SWE in forest sites. The interception of rainfall in the snowpack (LWDR) has also a positive impact on forest sites simulations, while keeping the open plots unchanged. The changed albedo formulation (LWDR_AFA) shows a significant improvement in open sites, with a small impact on forest sites. When all the new components are activated (NEW) the RMSE of SWE is lower than any of the other experiments in both open and forest sites. Open sites had a delayed ablation in CTR, which was mainly reduced with the new exposed albedo formulation. The early ablation in forest sites was corrected mainly due to the incorporation of SLW.

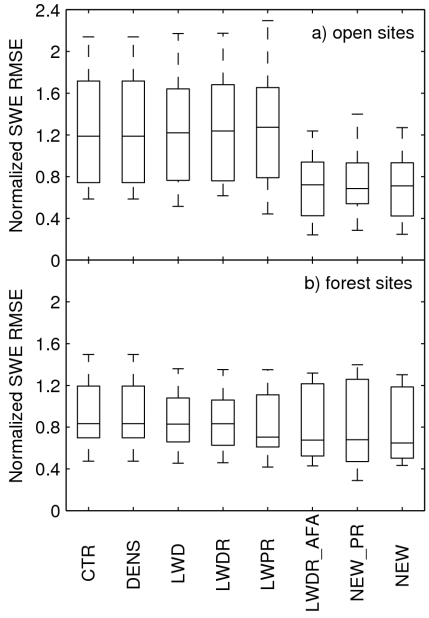

Fig. 4 Box plot summaries describing the normalized root mean square error (RMSE) of SWE for different model configurations, combined at all SNOWMIP2 locations at open sites (a) and forest sites (b). The boxes have horizontal lines at the lower quartile, median and upper quartile and the whiskers (vertical lines) extend from the end of each box to 1.5 times the interquartile range.

SLW is often represented in snow schemes following a prognostic approach. The experiments LWPR and NEW_PR were conducted to analyze the impact of such approach, when compared to the diagnostic implementation described in this report. This simple validation aims to examine whether or not the approaches are comparable, not to decide which one is better. The RMSE of SWE in LWPR is comparable with LWDR for forest sites, but LWPR has a better performance than LWDR in open plots. On the other hand, the inclusion of all physical mechanisms in NEW_PR dilutes the advantages of the prognostic water reservoir.

4 Basin scale validation

4.1 Simulations setup

GSWP2 provides a set of near-surface forcing to drive land surface schemes in an offline mode. The atmospheric forcing data are provided at a resolution of 1° globally. In the current work, we have used the latest release of GSWP2 atmospheric forcing based in the ERA-40 reanalysis (Uppala et al. 2005) where only precipitation is corrected using the Global Precipitation Climatology Project (GPCP) dataset. The dataset is available for the period January 1986 to December 1995. Surface pressure, air temperature and specific humidity at 2-m, and wind at 10-m are provided as instantaneous values. Downward surface radiation fluxes and precipitation fluxes represent 3-hour averages. Climatological data, such as land cover and vegetation types, were interpolated to a 1º×1º degree grid from the ECMWF ERA-40 reanalysis.

4.2 Basins and observations

Terrestrial water storage is the sum of all forms of water storage on the land surface. Seasonal and interannual variations in storage are determined by the combined effect of soil moisture, groundwater, snow cover and surface water. Diagnostics of monthly TWSV for 41 mid-latitude basins all over the globe were used to validate the new snow scheme. The Basin Scale Water Balance (BSWB) dataset described in Hirschi et al. (2006) was derived with the combined atmospheric and terrestrial water-balance approach (Seneviratne et al. 2004) using conventional streamflow measurements and vertically integrated atmospheric moisture convergence data from ERA-40. The runoff data is partially composed of data from the Global Runoff Data Centre (GRDC) and other local sources. In the following discussion HTESSEL simulations were spatially aggregated for each basin.

Such large-scale basins are composed by many types of land cover, rivers and lakes, each one with different hydrological characteristics. Simulated integrated values such as runoff and TWSV were spatially averaged. This simple procedure neglects river routing and effects of water and soil freezing. Such processes may delay basin streamflow, when compared with instantaneous local runoff. However, the BSWB dataset consists of monthly data, which are compared against time averaged monthly simulated fluxes. This approach has been also used by Balsamo et al. (2009) during the validation of HTESSEL soil hydrology.

4.3 Impact in the Ob basin

The Ob River is a major river in western Siberia, Russia. The basin consists mostly of steppe, taiga, swamps, tundra and semi-desert, with an average high vegetation fraction of 50%. Simulated SWE, snow density, percentage of frozen surface and runoff are presented in Fig. 5 for the 1989-1990 period. SWE simulated by the new snow scheme is higher than in CTR (Fig. 5a). The interception of rainfall in the snowpack was 53 mm while snowfall was 218 mm. The additional accumulation of 53 mm to the snowpack in NEW explains the differences in SWE, resulting in a 14 days difference during final ablation between NEW and CTR. As

for the SnowMIP2 sites, snow density is lower in NEW throughout the winter, reaching higher values than CTR only during the ablation period.

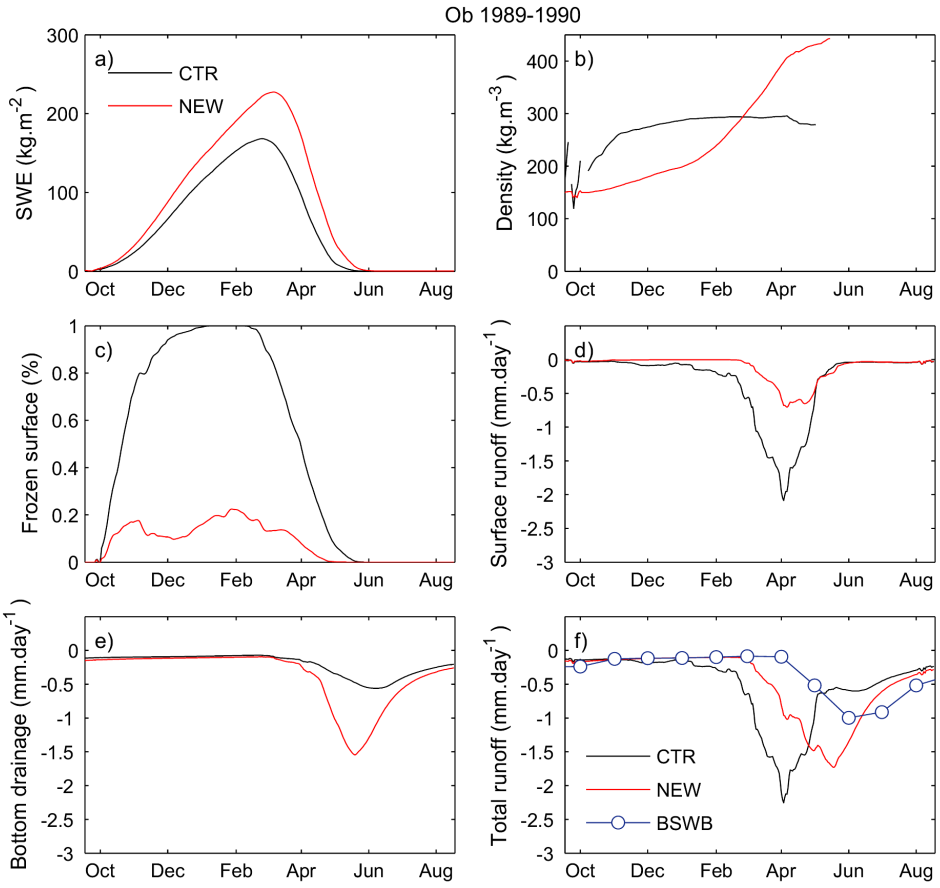

Fig. 5 Simulation results for CTR (in black) and NEW (in red) during the period October 1989 to August 1990 spatially averaged for the Ob basin: (a) SWE; (b) snow density; (c) fraction of basin area frozen at the surface; (d) surface runoff; (e) bottom drainage and (f) total runoff. Total runoff simulations are compared with monthly BSWB data. Simulated daily data were smoothed with a 30-days moving average.

Lower snow density and higher SWE result in a thicker snowpack, with an increased insulation effect. The percentage of frozen soil in Fig 5c is the fractional basin area where the first soil layer (0-7 cm) is frozen. The increased insulation in NEW reduces soil cooling, which reduces soil freezing. In CTR the basin surface is completely frozen from January to mid February, while in NEW only 20% to 30% of the basin is frozen. The runoff partitioning between surface and bottom drainage is shifted in NEW with a reduction of surface runoff (Fig. 5d), and an increase of bottom drainage (Fig. 5e). In HTESSEL all rainfall and melted water are discharged as surface runoff when the first soil layer is frozen. The NEW snow scheme reduces soil freezing, therefore reducing surface runoff and increasing soil water storage. The overall impact in total runoff is represented in Fig. 5f where NEW and CTR are compared against BSWB monthly data. The peak runoff date is accelerated and volume overestimated by CTR and NEW. However, the NEW snow scheme improves both the timing and magnitude of the total basin runoff.

4.4 Monthly TWSV and Runoff

Figure 6 compares the mean annual cycles of simulated runoff and TWSV with BSWB data over Ob and Mackenzie basins. The mean annual cycles of CTR runoff show an early peak in both basins with overestimation in the Ob, but with a correct volume in Mackenzie. Both timing and volume are improved in NEW over the Ob basin (as discussed before), while the volume in the Mackenzie is poorer than in CTR. The simulated TWSV in CTR displays timing errors similar to the runoff in both basins. The increased water storage during spring in NEW resulted in a better agreement with BSWB TWSV during summer. The reduction of total runoff in both basins in NEW was compensated by an increase in evapotranspiration, especially during spring (not shown). Less soil freezing and early thaw increase evapotranspiration in NEW, since more water is available for the plant root uptake.

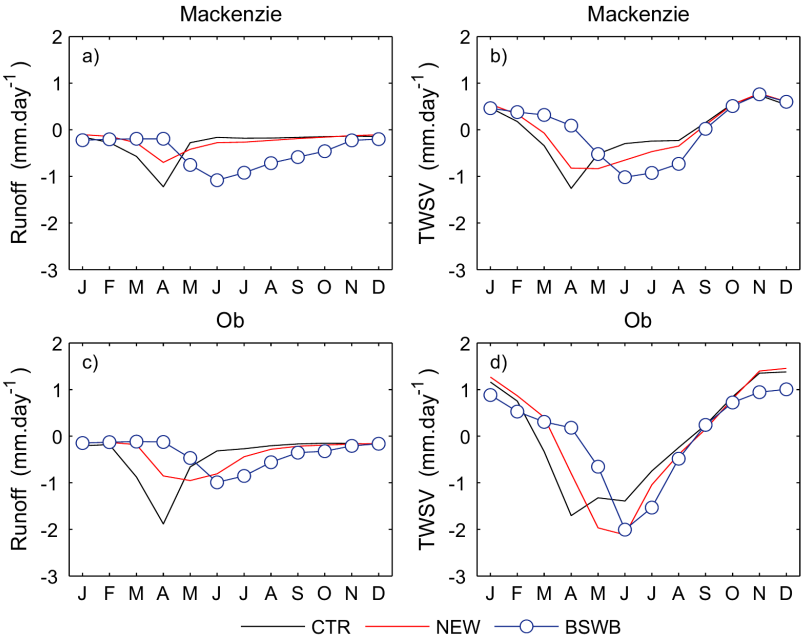

Fig. 6 Mean annual cycles of runoff (a,c) and TWSV (b,d) in Mackenzie and Ob basins simulated by CTR and NEW during GSWP-2 period and compared with BSWB data.

Table 3 summarizes the RMSE of runoff in ten high-latitude basins, corresponding to the subset of the original 41 basins of the BSWB dataset where more than 30% of available data has mean snow cover duration exceeding 100 days. The mean snow cover duration was calculated for all grid-points, and then averaged for each basin, using the CTR simulation. For all the basins with snow cover duration less than 100 days the differences between CTR and NEW are negligible. This result is due to the smaller impact of snow in the hydrological cycle.

The last two columns of table 3 compare the runoff RMSE between the diagnostic (LWDR) and the prognostic (LWPR) formulation to represent SLW. The differences between the two formulations are small. The inclusion of the new snow cover fraction, exposed albedo and forest albedo (NEW) to LWDR also shows a small effect in the runoff. The similar performance of NEW, LWDR and LWPR, very distinct from CTR is an indication that the new snow density is the most important change. As discussed before, the original scheme suffered from a lack of soil water storage due to excessive surface runoff. Averaged over all ten basins, NEW reduces the runoff RMSE by 0.24 mm day-1 (32 % of the CTR). With the exception of the Neva river basin, any of the three new formulations performs better than CTR.

Table 3. Root Mean Square Error (RMSE) of simulated versus BSWB runoff in 10 high latitude basins. Simulations forced by GSWP2 for the period 1986-1995. For each basin are presented the catchment area (adapted from Hirschi et al. 2006), mean snow cover duration and mean annual amplitude of runoff.

Basin	Catchment area (km^2)	Snow duration (days)	Runoff ($mm\ day^{-1}$)	Runoff RMSE ($mm\ day^{-1}$)			
				CTR	NEW	LWDR	LWPR
Yukon	779 081	198	2.18	0.95	0.53	0.58	0.58
Podka.[a]	209 591	190	3.47	0.90	0.45	0.50	0.57
Lena	2 351 052	182	3.07	0.96	0.84	0.86	0.87
Tom	62 830	158	6.92	1.88	1.59	1.68	1.64
Ob	2 859 889	154	1.06	0.69	0.32	0.34	0.38
Yenisei	2 513 361	151	2.79	0.77	0.46	0.51	0.54
Mackenzie	1 587 878	140	1.34	0.55	0.42	0.45	0.44
Volga	1 333 747	137	1.16	0.65	0.53	0.55	0.57
Irtish	403 309	129	0.41	0.42	0.22	0.21	0.25
Neva	233 423	116	0.80	0.60	0.63	0.64	0.63
Average[b]	12 334 161[c]	157	1.96	0.75	0.51	0.54	0.56

[a]- Podkamennaya Tunguska
[b]- Average weighted by catchment area
[c]- Total catchment area

5 Global validation

5.1 Simulation setup

ERAI reanalysis covers the period January 1989 to present. The atmospheric forcing data were gridded on the original Gaussian reduced grid N128 (resolution of 0.7° over the equator) globally at three-hour intervals. The state variables are provided as instantaneous values from the lowest model level (approximately 10-m above the surface), and correspond to the 3-12h forecast interval from initial conditions at 00 and 12 UTC. Surface precipitation and radiation fluxes represent 3-hour averages. To avoid the initial spin-up in precipitation, the three-hourly surface fluxes are taken from the 9h to 21h forecasts initialized at 00 and 12 UTC.

Unlike GSWP2, ERAI precipitation was not corrected with GPCP (or other) observational dataset. Errors in total precipitation and partitioning between liquid and solid rainfall may produce biases in the simulated snowpack. Such corrections are out of the scope of the present work. Nevertheless, the ERAI dataset has already been explored in offline LSM works (Balsamo et al. 2009a, Dutra et al. 2009). Dutra et al. (2009) showed that HTESSEL forced in stand-alone mode with ERAI produces global evapotranspiration fields similar to the reanalysis.

5.2 Snow cover

5.2.1 IMS NOAA/NESDIS snow cover

The interactive Multisensor Snow and Ice Mapping System (IMS) is a workstation based application, which allows the analyst to process various snow-cover data in a manner timely enough to release a real-time daily product (Helfrich et al. 2007, Ramsay 1998). Northern Hemisphere (NH) snow-covered maps are primarily

based on satellite imagery. In addition, the analyst can rely on station data and the previous day's analysis. Since February 1997, the IMS product has been produced daily at approximately 24 km resolution (1024 × 1024 grid). This dataset has already been applied to the validation of model-simulated snow cover extent in other studies (e.g. Sheffield et al. 2003). IMS NOAA/NESDIS snow cover product (NOAA/NESDIS/OSDPD/SSD 2004, updated 2006) was spatially aggregated to the N128 Gaussian reduced grid. Fractional snow cover in the Gaussian grid was evaluated from the original "snow free/100% snow-covered" binary information. Snow cover fraction was calculated by counting all the 100% snow-covered pixels of NOAA/NESDIS lying within each N128 grid-box.

5.2.2 Snow cover simulations

NH simulated snow-covered area is compared against NOAA/NESDIS in Fig. 7. Snow-covered area maximum extents exceed 40 million km^2, which is coherent with the results presented by Brown and Armstrong (2008). The differences between simulated and NOAA/NESDIS (Fig. 7.) show a distinct annual cycle. The bias is reduced during low variability periods, namely summer and late winter. On the other hand, the bias is higher during the high variability accumulation and ablation seasons. During the initial accumulation period both CTR and NEW show a growing underestimation of snow-cover area, that reaches roughly 6 million km^2. After the initial accumulation, NEW reduces the bias significantly near the peak snow-covered area. During spring both schemes tend to ablate snow cover too quickly, with increasing underestimation. This behavior was also documented by Frei et al. (2005) in the AGCMs participating in AMIP-2. Averaged over the entire period (January 1999 to December 2008) CTR and NEW have a negative bias in snow-covered area of 3.1 and 1.6 million km^2, respectively. During spring, CTR and NEW biases are higher: 5.3 and 2.6 million km^2. LWDR_SC simulation partially reduces the bias of CTR, showing that the new snow cover fraction (eq. 12) has an important effect in the model-simulated snow cover extent.

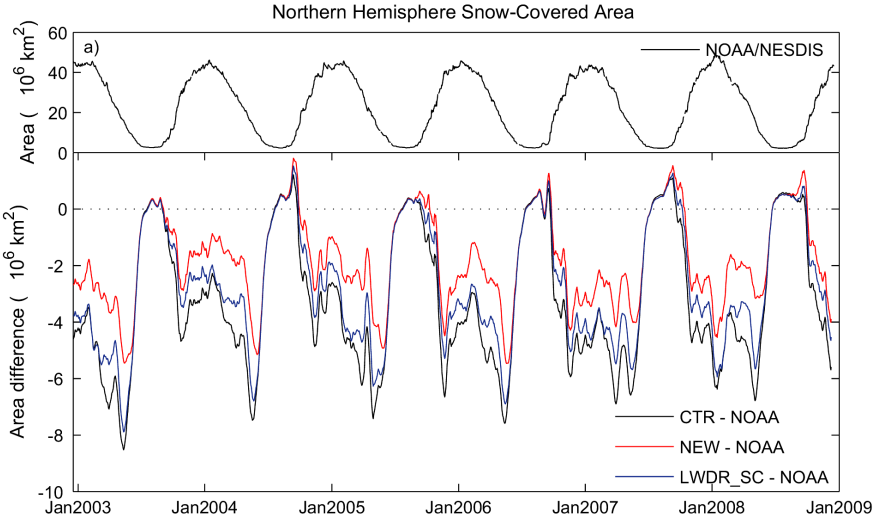

Fig. 7 Northern Hemisphere daily snow-covered area from NESDIS (a), and snow-covered area differences between simulations and NESDIS (b). Note the different order of magnitude in the vertical axis between the two panels.

The NOAA/NESDIS data is a daily product allowing for a more detailed comparison with simulations. Figure 8 presents the spatial distribution of the frequency of missing snow cover in the simulations during spring, defined as the frequency of occurrence of snow-covered NOAA/NESDIS (c_{sn}>0.75) and simulated snow-free (c_{sn}<0.25). Drusch et al. (2004) applied a similar diagnostic to validate the snow depth analysis system in ECMWF. Scandinavia, western Russia and central/eastern Canada are dominated by high frequency snow cover missing in CTR (Fig 8a), reaching one month (30%) in some localized areas. These results agree with the pronounced underestimation of snow-covered area during spring in CTR, analyzed before. NEW reduces the missing snow cover during spring, when compared with the CTR up to a factor of two in areas where CTR has higher errors.

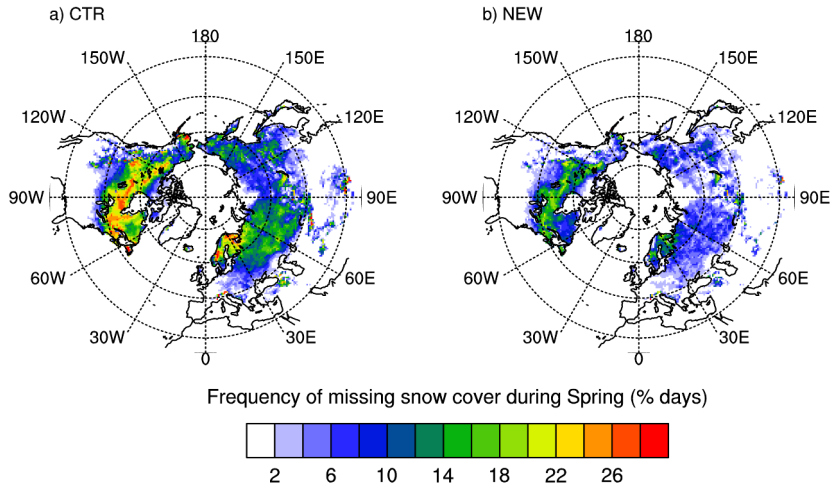

Fig. 8 Frequency of occurrence of snow-covered NESDIS data (c_{sn}>0.75) and simulated snow-free (c_{sn}>0.75) during spring (March-April-May) for ERAI simulations in the period 2001-2008 by CTR (a) and NEW (b). The number of days in each grid box is normalized by the total number of days of the season.

5.3 Surface albedo

5.3.1 MODIS albedo

The MODIS albedo product MCD43C3 provides data describing both directional hemispheric reflectance (black-sky albedo) and bihemispherical reflectance (white-sky albedo). Both black-sky and white-sky albedos are available in seven different bands and aggregated visible, near infrared and broad band shortwave. Both Terra and Aqua platforms are used in the generation of this product. The product also includes snow-free and quality parameters, and is produced every 8 days with 16 days of acquisition projected to a 0.05° grid. These data are distributed by the Land Processes Distributed Active Archive Center (LP DAAC), located at the U.S. Geological Survey (USGS) Earth Resources Observation and Science (EROS) Center (lpdaac.usgs.gov). The accuracy and quality of this albedo product have been evaluated by Stroeve et al. (2005), Salomon et al. (2006), Shuai et al. (2008) and Román et al. (2009). The white-sky broadband shortwave albedo was spatially aggregated from the original 0.05° grid to the N128 Gaussian reduced grid.

5.3.2 Albedo simulations

Figure 9a compares simulated albedo against MODIS-derived albedo in the snow-covered area in the NH. In the following discussion, snow-covered area was derived from the MODIS Percent_Snow layer. Therefore, the mean fractional land area with available data (see top of each graphic in Fig. 9) excludes snow-free

MODIS grid-boxes and also missing data (e.g. due to cloud cover or low quality of the albedo inversion algorithm).

CTR albedo shows a systematic negative bias that increases in magnitude throughout the cold season until May. The exposed albedo parameterization by itself (LWDR_A) improves the simulation in all months except October. The new lookup table for shaded snow (LWDR_FA) has a positive impact in all months. The NEW snow scheme significantly reduces the albedo bias in all months except October and November. During these two months the signal shift of the albedo bias (from negative in CTR to positive in NEW) and increased magnitude is due to the new exposed albedo parameterization (compare LWDR_A with LWDR_FA in Fig. 9a). Groisman et al. (1994b) showed that the impact of snow cover in the planetary albedo has the greatest magnitude in spring. Therefore, the degradation of simulated albedo in NEW during late autumn should have a smaller impact then the improvements during late winter and spring. The new snow cover fraction by itself (LWDR_SC) has similar results to CTR, showing that the improved simulated albedo is mainly due to the modified exposed and shaded snow parameterizations.

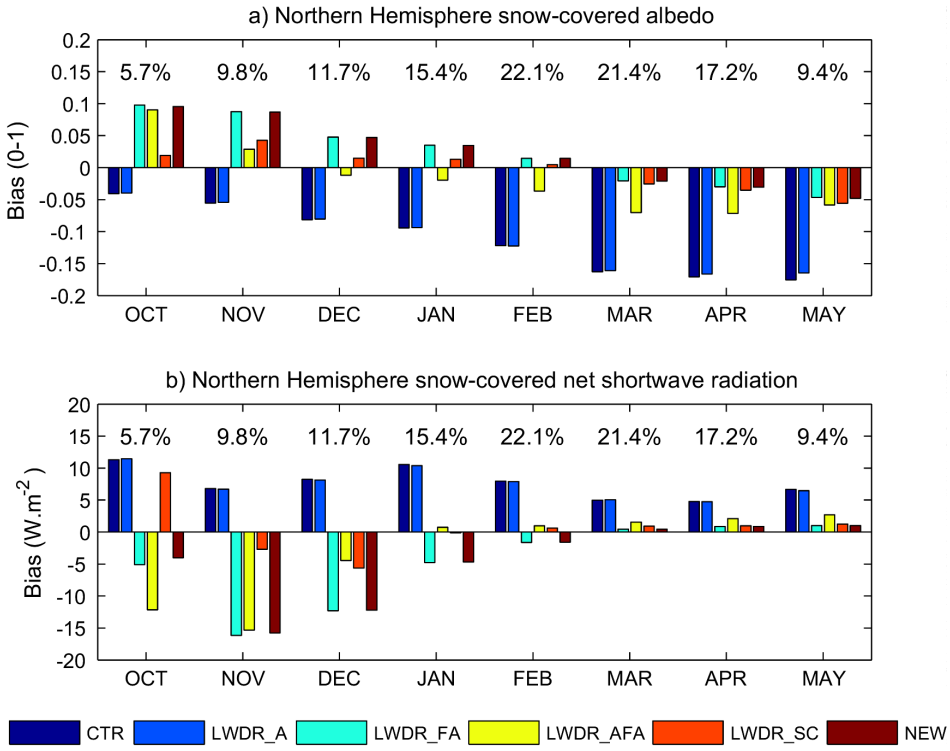

Fig. 9 Monthly bias (simulation-observation) of albedo (a) and net shortwave radiation (b) calculated only over snow-covered grid-boxes over the northern hemisphere. The fractional snow-covered land of Northern Hemisphere used in the calculations for each month is presented in the top of each graphic. ERAI simulations of albedo and net shortwave radiation are compared against MODIS albedo for the period January 2000 to December 2008.

The impact of albedo biases on the snowpack is modulated by the amount of available solar radiation. Net shortwave radiation (SWnet) is not a direct MODIS product. It was diagnosed using MODIS albedo and ERAI downward shortwave radiation and is compared against simulations in Fig. 9b. The above mentioned CTR albedo negative bias is reflected in a positive SWnet bias during the entire snow-covered season. On the other hand, NEW SWnet bias is close to zero during late winter and spring, but with a negative bias in November and December. The reasons for this bias were discussed before. Averaged results from October to May and weighted by the snow-covered area, CTR has a mean positive bias of +7.1 W m^{-2}, while NEW has a

mean negative bias of -1.9 W m^{-2}. In absolute terms, NEW reduces the SWnet bias by 5.2 W m^{-2} when compared with CTR. The area where such flux differences are found cover 14% of the NH land.

Figure 10 represents the mean (2000-2008) spring MODIS albedo and respective simulated differences. The differences between simulated and MODIS albedo (Fig. 10b,c) are shown only for snow-covered grid-boxed flagged by MODIS with at least 50% of feasible data (excluding areas with systematic missing values in MODIS). The negative bias of CTR albedo (see also Fig. 9a) during spring spreads widely over the entire northern hemisphere. There are three main regions with an accentuated bias: Northeast Asia, Central Asia (north of Caspian and Aral Seas) and Northern Canada. These areas are dominated by low vegetation (tundra and short grass). NEW partially reduces the albedo bias over low vegetation areas while over high vegetation areas the bias is close to zero. There are some small positive biases in NEW on the southern borders of tundra regions (areas dominated by bogs and marshes) in both continents.

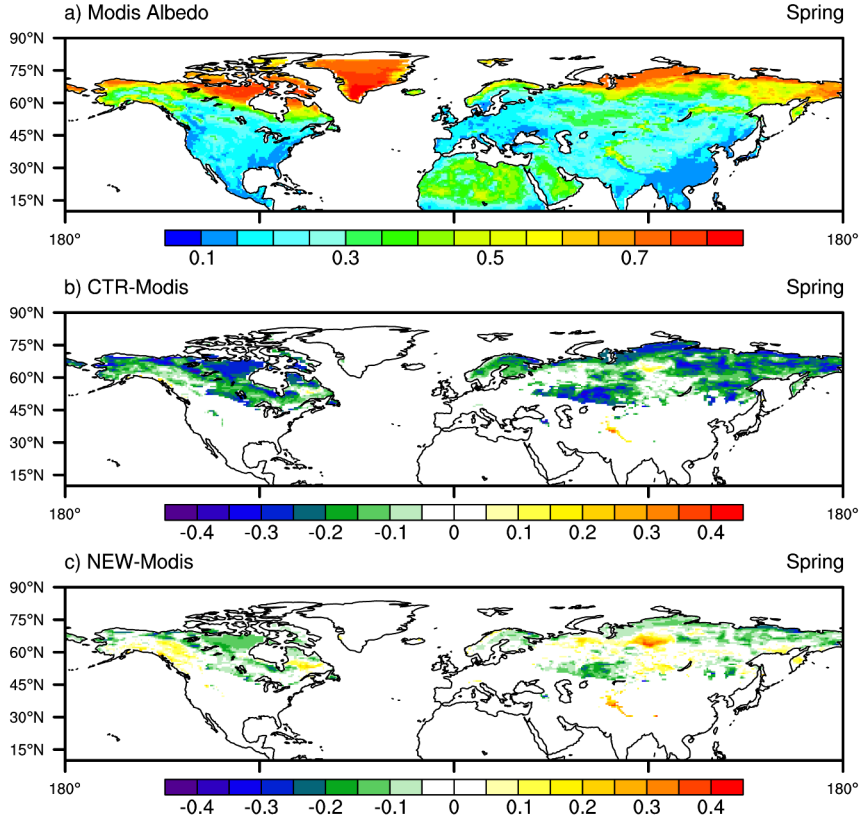

Fig. 10 Mean observed maps of spring albedo by MODIS for the period 2000-2008 (a) and differences between simulated albedo and MODIS (b) and (c) for CTR and NEW respectively. The differences panels (b and c) show only snow-covered grid-boxes with less than 50% MODIS missing data. Note the different colour scales between panel a) and panels b) and c).

6 Conclusions

An improved snow scheme for HTESSEL was presented and validated. The new scheme revises the formulations of snow cover fraction and snow albedo, and included a new snow density parameterization and representation of SLW using a diagnostic approach. An offline validation covering several spatial and temporal scales considered (i) site simulations for several observational locations from SnowMIP2 and (ii) global simulations driven by the meteorological forcings from GSWP2 and ERAI.

SnowMIP2 simulations revealed that the original snow scheme had a systematic early and late prediction of the final ablation in forest and open sites, respectively. The NEW scheme reduces the negative timing bias in forest plots from 21 to 13 days and the positive bias in open plots from 10 to 2 days. The new snow density parameterization in NEW has a good agreement with observations, resulting in an augmented insulation effect of the snowpack. The increased insulation and the new exposed and shaded albedo change the surface energy fluxes. There is a reduction of the basal heat flux that reduces the cooling of the underlying soil, which is warmer in NEW than in CTR during the cold season. Thus, reduced soil freezing decreased the surface runoff and increased soil water storage. The mean annual cycles of runoff and TSWV analyzed for the Ob and Mackenzie basins are closer to the observations in NEW. In ten Northern hemisphere basins, there is an average reduction of the monthly runoff RMSE from 0.75 to 0.51 mm day^{-1} when comparing CTR and NEW, respectively. These results illustrate the importance of the snow insulation on the hydrological cycle, even at regional scales.

On a hemispheric scale, the new snow scheme reduces the negative bias of snow-covered area, especially during spring. On a daily scale, using NOAA/NESDIS snow cover data, the early ablation in CTR is reduced by a factor of two in some identified regions over the Northern Hemisphere. The changes in snow-covered area are closely related with the changes in surface albedo. The original snow scheme had a systematic negative bias in surface albedo, when compared against MODIS remote sensing data. The new scheme reduced the albedo bias, consequently reducing the spatial (only over snow covered area) and time (October to November) averaged surface net shortwave radiation bias from +7.1 W m^{-2} in CTR to -1.8 W m^{-2} in NEW.

For each validation dataset, sensitivity experiments were performed to assess the impact of the new components of the presented snow scheme. Prognostic and diagnostic SLW representations display similar skill in SnowMIP2 (RMSE of SWE) and GSWP2 (RMSE of basin runoff) simulations. Simulated improvements of SWE in SnowMIP2 locations were mainly due to SLW representation on forest sites and due to the new exposed albedo on open sites. The increased snow insulation effect, due to the new snow density parameterization, had an important role on the basins water balance. Impacts of the new snow cover fraction and exposed and shaded albedo parameterizations were evident when validating against remotely sensed data. Sensitivity tests highlight the role of the different components of the snow scheme with the behavior conditioned by the climate and vegetation conditions of each site. Thus, a robust verification of a LSM model should include a variety of different (and independent) validation datasets.

The present offline methodology is recurrent in validations of LSM (e.g. Boone and Etchevers 2001) and in intercomparison projects (e.g. Rutter et al. 2009). However, the associated nature of the one-way coupling has shortcomings due to the absence of atmospheric response. A complete validation can only be achieved with atmospherically coupled simulations. Tests have been performed and the new snow scheme showed improvements in the simulated near-surface temperature during winter over snow-covered areas; such results will be reported in future work. Future developments of HTESSEL snow scheme will focus on improvements of the physics representation of the snowpack (e.g. development of a multi-layer scheme), and on the coupling with the atmosphere, especially in forested regions. The NEW snow scheme described in this report was introduced in the ECMWF operational forecast system in September 2009 (CY35R3).

Acknowledgments

The authors would like to thank SnowMIP2 data providers: David Gustafsson and Manfred Stähliand (Alptal – Switzerland); Alan Barr and Paul Bartlett (Berms – Canada); Kazuyoshi Suzuki and Tomoyoshi Hirota (Hitsujigaoka – Japan); Nuria Altimir and Timo Vesala (Hyytiälä – Finland); and Richard Essery and Nick Rutter for the project organization and useful comments. The BSWB dataset was kindly provided by Martin Hirschi. We also thank the MODIS Land and Albedo teams and in particular Crystal Schaaf for the valuable support and comments regarding the use of MODIS albedo product.This work was supported by the Portuguese Foundation for Science and Technology (FCT) under project AMIC PTDC/AAC-CLI/109030/2008 cofinanced by the European Union under program FEDER. E. Dutra acknowledges the financial support of FCT under grant SFRH/BD/35789/2007 and Fundação Calouste Gulbenkian.

APPENDIX

HTESSEL snow scheme

The snow mass budget read as

$$\frac{\partial S}{\partial t} = F - c_{sn} E_{sn} - M_{sn} \tag{A.1}$$

where the symbols are defined in section 2.1. The snow fraction is given by:

$$c_{sn} = \min\left(1, \frac{S}{15}\right) \tag{A.2}$$

Snow mass and snow depth are related by

$$D_{sn} = \frac{S}{\rho_{sn} c_{sn}} \tag{A.3}$$

where D_{sn} is snow depth (m) in the snow-covered area (D_{sn} is not a grid-averaged quantity).

The snow energy budget read as

$$\left(\rho C\right)_{sn} D_{sn} \frac{\partial T_{sn}}{\partial t} = R_{sn}^{N} - L_s E_{sn} - H_{sn} - G_{sn}^{B} - L_f M_{sn} \tag{A.4}$$

In this formulation the liquid water fraction is neglected. The snow thermal conductivity changes with changing snow density and is related to the ice thermal conductivity according to Douville et al. (1995).

Following Douville et al. (1995) snow density is assumed to be constant with depth and to evolve exponentially towards a maximum density (Verseghy 1991). First a weighted average is taken between the current density (current snow mass) and the minimum density for fresh snow (mass of snowfall), and after is applied an exponential relaxation

$$\rho_{sn}^{t+1} = \left(\rho_{sn} - \rho_{sn_{\max}}\right)\exp\left(-\tau_f \, \Delta t/\tau_1\right) + \rho_{sn_{\max}} \tag{A.5}$$

where τ_1=86400 s, and τ_f=0.24 are timescales, with minimum density $\rho_{sn_{\min}}$=100 kg m^{-3} and maximum density $\rho_{sn_{\max}}$=300 kg m^{-3}.

Snow albedo in exposed areas evolves according to the formulation of Baker et al. (1991), Verseghy (1991) and Douville et al. (1995) differing for melting and non-melting conditions:

$$\alpha_{sn}^{t+1} = \begin{cases} \alpha_{sn}^{t} - \tau_a \, \Delta t/\tau_1 & , M_{sn} = 0 \\ \left(\alpha_{sn}^{t} - \alpha_{\min}\right)\exp\left(\tau_f \, \Delta t/\tau_1\right) + \alpha_{\min} & , M_{sn} > 0 \end{cases} \tag{A.6}$$

where α_{min}=0.5 and α_{max}=0.85. If snowfall F>1 kg m^{-2} h^{-1}, the snow albedo is reset to the maximum value. The albedo for shaded snow is fixed at 0.15. A detailed description of the scheme can be found at http://www.ecmwf.int/research/ifsdocs/CY28r1/Physics/index.html.

References

Anderson, E.A., 1976: A point energy and mass balance model of a snow cover. NOAA Tech. Rep. , NWQ 19, 150 pp.

Armstrong, R.L. and Brun, E., Eds., 2008: Snow and Climate. Physical processes, surface energy exchange and modeling. Cambridge University press, 222 pp.

Baker, D.G., Skaggs, R.H. and Ruschy, D.L., 1991: Snow Depth Required to Mask the Underlying Surface. *J. Appl. Meteorol.*, 30, 387-392.

Balsamo, G., Dutra, E., Stepanenko, V.M., Viterbo, P., Miranda, P.M.A. and Mironov, D.V., 2010: Deriving an effective lake depth from satellite lake surface temperature data: A feasibility study with MODIS data. *Bor. Environ. Res.*, in press.

Balsamo, G., Viterbo, P., Beljaars, A., Van den Hurk, B., Betts, A.K. and Scipal, K., 2009: A revised hydrology for the ECMWF model: Verification from field site to terrestrial water storage and impact in the Integrated Forecast System. *J. Hydrometeorol.*, 10, 623-643.

Bélair, S., Brown, R., Mailhot, J., Bilodeau, B. and Crevier, L.P., 2003: Operational implementation of the ISBA land surface scheme in the Canadian regional weather forecast model. Part II: Cold season results. *J. Hydrometeorol*, 4, 371-386.

Boone, A. and Etchevers, P., 2001: An intercomparison of three snow schemes of varying complexity coupled to the same land surface model: Local-scale evaluation at an alpine site. *J. Hydrometeorol*, 2, 374-394.

Boone, A. and Coauthors, 2004: The Rhone-aggregation land surface scheme intercomparison project: An overview. *J. Climate*, 17, 187-208.

Brown, R. and Armstrong, R.L., 2008: Snow-cover data: measurement, products, and sources. Snow and Climate, R.L. Armstrong and E. Brun, Eds., Cambridge University Press,181-216.

Brun, E., David, P., Sudul, M. and Brunot, G., 1992: A Numerical-Model to Simulate Snow-Cover Stratigraphy for Operational Avalanche Forecasting. *J. Glaciol.*, 38, 13-22.

Brun, E., Martin, E., Simon, V., Gendre, C. and Coleou, C., 1989: An Energy and Mass Model of Snow Cover Suitable for Operational Avalanche Forecasting. *J. Glaciol.*, 35, 333-342.

Cohen, J., Barlow, M., Kushner, P.J. and Saito, K., 2007: Stratosphere-troposphere coupling and links with Eurasian land surface variability. *J. Climate*, 20, 5335-5343.

Cook, B.I., Bonan, G.B., Levis, S. and Epstein, H.E., 2008: The thermoinsulation effect of snow cover within a climate model. *Climate Dyn.*, 31, 107-124.

Dirmeyer, P.A., Dolman, A.J. and Sato, N., 1999: The pilot phase of the Global Soil Wetness Project. *Bull. Am. Meteorol. Soc.*, 80, 851-878.

Dirmeyer, P.A., Gao, X. and Oki, T., 2002: The second global soil wetness project science and implementation plan. International GEWEX project Office Publication Series, Vol. 37, IGPO, 75pp.

Douville, H., Chauvin, F., Planton, S., Royer, J.F., Salas-Melia, D. and Tyteca, S., 2002: Sensitivity of the hydrological cycle to increasing amounts of greenhouse gases and aerosols. *Climate Dyn.*, 20, 45-68.

Douville, H. and Royer, J.F., 1996: Sensitivity of the Asian summer monsoon to an anomalous Eurasian snow cover within the Meteo-France GCM. *Climate Dyn.*, 12, 449-466.

Douville, H., Royer, J.F. and Mahfouf, J.F., 1995: A New Snow Parameterization for the Meteo-France Climate Model .1. Validation in Stand-Alone Experiments. *Climate Dyn.*, 12, 21-35.

Drusch, M., Vasiljevic, D. and Viterbo, P., 2004: ECMWF's global snow analysis: Assessment and revision based on satellite observations. *J. Appl. Meteorol.*, 43, 1282-1294.

Dutra, E., Stepanenko, V.M., Balsamo, G., Viterbo, P., Miranda, P.M.A., Mironov, D.V. and Schär, C., 2010: An offline study of the impact of lakes on the performace of the ECMWF surface scheme. *Bor. Environ. Res.*, in press.

Essery, R., and Coauthors, 2009: SnowMIP2 An evaluation of forest snow process simulations. *Bull. Am. Meteorol. Soc.*, 90, 1120-1135.

Fletcher, C.G., Hardiman, S.C., Kushner, P.J. and Cohen, J., 2009: The Dynamical Response to Snow Cover Perturbations in a Large Ensemble of Atmospheric GCM Integrations. *J. Climate*, 22, 1208-1222.

Frei, A., Brown, R., Miller, J.A. and Robinson, D.A., 2005: Snow mass over North America: Observations and results from the second phase of the atmospheric model intercomparison project. *J. Hydrometeorol.*, 6, 681-695.

Gao, X., Dirmeyer, P.A. and Oki, T., 2004: Update on the second global soil wetness project (GSWP-2). GEWEX Newsletter, Vol. 14, No 3, International.GEWEX Project Office, Silver Spring, MD, 10.

Gong, G., Cohen, J., Entekhabi, D. and Ge, Y., 2007: Hemispheric-scale climate response to Northern Eurasia land surface characteristics and snow anomalies. *Global Planet. Change*, 56, 359-370.

Grippa, M., L. Kergoat, T. Le Toan, N. M. Mognard, N. Delbart, J. L'Hermitte, and S. M. Vicente-Serrano, 2005: The impact of snow depth and snowmelt on the vegetation variability over central Siberia, *Geophys. Res. Lett.*, 32, L21412, doi:10.1029/2005GL024286

Groisman, P.Y., Karl, T.R. and Knight, R.W., 1994a: Observed Impact of Snow Cover on the Heat-Balance and the Rise of Continental Spring Temperatures. *Science*, 263, 198-200.

Groisman, P.Y., Karl, T.R., Knight, R.W. and Stenchikov, G.L., 1994b: Changes of Snow Cover, Temperature, and Radiative Heat-Balance over the Northern-Hemisphere. *J. Climate*, 7, 1633-1656.

Groisman, P.Y., Knight, R.W., Karl, T.R., Easterling, D.R., Sun, B.M. and Lawrimore, J.H., 2004: Contemporary changes of the hydrological cycle over the contiguous United States: Trends derived from in situ observations. *J. Hydrometeorol.*, 5, 64-85.

Helfrich, S.R., McNamara, D., Ramsay, B.H., Baldwin, T. and Kasheta, T., 2007: Enhancements to, and forthcoming developments in the Interactive Multisensor Snow and Ice Mapping System (IMS). *Hydrol. Process.*, 21, 1576-1586.

Hirschi, M., Seneviratne, S.I. and Schar, C., 2006: Seasonal variations in terrestrial water storage for major midlatitude river basins. *J. Hydrometeorol.*, 7, 39-60.

Jordan, R., 1991. A one-dimensional temperature model for snow cover. CRREL special Rep. 91-b, Cold Regions Research and Engeneering Laboratory, Hanover, 49 pp.

Liu, X.D. and Yanai, M., 2002: Influence of Eurasian spring snow cover on Asian summer rainfall. *Int. J. Climatol.*, 22, 1075-1089.

Loth, B., Graf, H.F. and Oberhuber, J.M., 1993: Snow Cover Model for Global Climate Simulations. *J. Geophys. Res.*, 98(D6), 10451-10464.

Lynch-Stieglitz, M., 1994: The Development and Validation of a Simple Snow Model for the Giss Gcm. *J. Climate*, 7, 1842-1855.

Molders, N., Luijting, H. and Sassen, K., 2008: Use of atmospheric radiation measurement program data from Barrow, Alaska, for evaluation and development of snow-albedo parameterizations. *Meteorol. Atmos. Phys.*, 99, 199-219.

Moody, E.G., King, M.D., Schaaf, C.B., Hall, D.K. and Platnick, S., 2007: Northern Hemisphere five-year average (2000-2004) spectral albedos of surfaces in the presence of snow: Statistics computed from Terra MODIS land products. *Remote Sen. Environ.*, 111, 337-345.

Nijssen, B. et al., 2003: Simulation of high latitude hydrological processes in the Torne-Kalix basin: PILPS phase 2(e) - 2: Comparison of model results with observations. *Global Planet. Change*, 38, 31-53.

NOAA/NESDIS/OSDPD/SSD, 2004, updated 2006: IMS daily Northern Hemisphere snow and ice analysis at 4 km and 24 km resolution. Boulder, CO: National Snow and Ice Data Center. Digital media. [Available online at: http://nsidc.org/data/g02156.html]

Pedersen, C.A. and Winther, J.G., 2005: Intercomparison and validation of snow albedo parameterization schemes in climate models. *Climate Dyn.*, 25, 351-362.

Ramsay, B.H., 1998: The interactive multisensor snow and ice mapping system. *Hydrol. Process.*, 12, 1537-1546.

Robock, A., Mu, M.Q., Vinnikov, K. and Robinson, D., 2003: Land surface conditions over Eurasia and Indian summer monsoon rainfall. *J. Geophys. Res.*, 108, 4131, doi:10.1029/2002JD002286.

Roesch, A. and Roeckner, E., 2006: Assessment of snow cover and surface albedo in the ECHAM5 general circulation model. *J. Climate*, 19, 3828-3843.

Román, M.O. and Coauthors, 2009: The MODIS (Collection V005) BRDF/albedo product: Assessment of spatial representativeness over forested landscapes. *Remote Sen. Environ.*, 113, 2476-2498.

Rutter, N., Cline, D. and Li, L., 2008: Evaluation of the NOHRSC snow model (NSM) in a one-dimensional mode. *J. Hydrometeorol.*, 9, 695-711.

Rutter, N., and Coauthors, 2009: Evaluation of forest snow processes models (SnowMIP2). *J. Geophys. Res.*, 114, D06111, doi:10.1029/2008JD011063.

Salomon, J.G., Schaaf, C.B., Strahler, A.H., Gao, F. and Jin, Y.F., 2006: Validation of the MODIS Bidirectional Reflectance Distribution Function and Albedo retrievals using combined observations from the Aqua and Terra platforms. *IEEE Trans. Geosci. Remote Sens.*, 44, 1555-1565.

Seneviratne, S.I., Viterbo, P., Luthi, D. and Schar, C., 2004: Inferring changes in terrestrial water storage using ERA-40 reanalysis data: The Mississippi River basin. *J. Climate*, 17, 2039-2057.

Sheffield, J. and Coauthors, 2003: Snow process modeling in the North American Land Data Assimilation System (NLDAS): 1. Evaluation of model-simulated snow cover extent. *J. Geophys. Res.*, 108, 8849, doi:10.1029/2002JD003274.

Shuai, Y.M., Schaaf, C.B., Strahler, A.H., Liu, J.C. and Jiao, Z.T., 2008: Quality assessment of BRDF/albedo retrievals in MODIS operational system. *Geophys. Res. Lett.*, 35, L05407, doi:10.1029/2007GL032568.

Simmons, A.J., Uppala, S.M., Dee, D. and Kobayashi, S., 2007: ERA-Interim: New ECMWF reanalysis product from 1989 onwards. ECMWF Newsletter, Vol 110, ECMWF, Reading, United Kingdom, 25-35.

Slater, A.G., Pitman, A.J. and Desborough, C.E., 1998: The validation of a snow parameterization designed for use in general circulation models. *Int. J. Climatol.*, 18, 595-617.

Stroeve, J., Box, J.E., Gao, F., Liang, S.L., Nolin, A. and Schaaf, C., 2005: Accuracy assessment of the MODIS 16-day albedo product for snow: comparisons with Greenland in situ measurements. *Remote Sens. Environ.*, 94, 46-60.

Sun, S.F., Jin, J.M. and Xue, Y.K., 1999: A simple snow-atmosphere-soil transfer model. *J. Geophys. Res.*, 104, 19587-19597.

Tribbeck, M.J., Gurney, R.J. and Morris, E.M., 2006: The radiative effect of a fir canopy on a snowpack. *J. Hydrometeorol.*, 7, 880-895.

Uppala, S.M., and Coauthors, 2005: The ERA-40 re-analysis. *Quart. J. Roy. Meteor. Soc.*, 131, 2961-3012.

van den Hurk, B. and Viterbo, P., 2003: The Torne-Kalix PILPS 2(e) experiment as a test bed for modifications to the ECMWF land surface scheme. *Global Planet. Change*, 38, 165-173.

van den Hurk, B., Viterbo, P., Beljaars, A.C.M. and Betts, A.K., 2000: Offline validation of the ERA-40 surface scheme. *ECMWF Tech. Memo.*, 295, 43 pp.

Verseghy, D.L., 1991: Class-a Canadian Land Surface Scheme for Gcms .1. Soil Model. *Int. J. Climatol.*, 11, 111-133.

Viterbo, P., Beljaars, A., Mahfouf, J.F. and Teixeira, J., 1999: The representation of soil moisture freezing and its impact on the stable boundary layer. *Q. J. Roy. Meteor. Soc.*, 125, 2401-2426.

Viterbo, P. and Beljaars, A.C.M., 1995: An Improved Land-Surface Parameterization Scheme in the Ecmwf Model and Its Validation. *J. Climate*, 8, 2716-2748.

Viterbo, P. and Betts, A.K., 1999: Impact on ECMWF forecasts of changes to the albedo of the boreal forests in the presence of snow. *J. Geophys. Res.*, 104, 27803-27810.

Yang, Z.L., Dickinson, R.E., Robock, A. and Vinnikov, K.Y., 1997: Validation of the snow submodel of the biosphere-atmosphere transfer scheme with Russian snow cover and meteorological observational data. *J. Climate*, 10, 353-373.